# Vapor-Liquid-Solid (VLS) Growth of Lead Chalcogenide Thin Films for Infrared Sensing Applications

by

Alexandra Andreevna Sourakov

Submitted to the
Department of Materials Science & Engineering
in Partial Fulfillment of the Requirements for the Degree of

Bachelor of Science

at the

Massachusetts Institute of Technology

June 2018



Signature redacted

Signature of Author .....
Department of Materials Science & Engineering
May 4, 2018

Signature redacted

Certified by.....
Rafael Jaramillo
Assistant Professor of Materials Science & Engineering
Thesis Supervisor

Signature redacted

Certified by.....
Juejun Hu
Associate Professor of Materials Science & Engineering
Chairman, Undergraduate Committee

# Abstract

Infrared sensors are used in a variety of applications, from gas and moisture analysers, to human body detection to spectrophotometers. Available IR technology falls on two ends of the spectrum: state-of-art photon detectors are high-quality but expensive and cumbersome due to the need for cryogenic cooling, while thermal detectors are inexpensive but not very sensitive. The goal of this project is to develop materials for uncooled IR sensors with improved performance. Lead selenide (PbSe) detectors are direct narrow band gap materials that have shown promise for relatively inexpensive IR sensing with modest cooling requirements. Adapting the vapour-liquid-solid (VLS) growth mechanism traditionally used for growing nanowires to growing PbSe thin films circumvents the very slow adsorption of a gas phase into a solid surface by introducing a catalytic liquid alloy phase, while simultaneously retaining the stoichiometric control, simplicity, and economy of vapor phase growth. We have set the stage for further experimentation by demonstrating that we can attain a single phase PbSe thin film via VLS growth on an epitaxially matched substrate. We have explored the effects of VLS growth vs. vapor growth on crystal quality as well as the factors that influence diffusion and nucleation rates, such as film thickness, growth temperature, and the presence of a capping layer.

# Acknowledgements

I would like to thank Professor Jaramillo for his mentorship and guidance throughout this project, as well as the whole Jaramillo Group for their support. I would particularly like to thank Anna and Yifei for their assistance with thermal evaporation; Stephen for helping me set up a protocol for growth experiments and helping to plan and execute the HF protocol; Seong Soon for her incredible patience in taking SEM images with me; Dr. Settens for his invaluable assistance with XRD analyses; Peter for a preliminary foray into Hall effect measurements; and Christophe for proofreading and providing comments.

# Table of Contents

# 1 Introduction

While attempting to develop a way to protect his eyes while looking at the sun, English astronomer Sir William Herschel, who was already well-known for his discovery of Uranus, discovered that there was a portion of radiant energy that existed well-beyond the visible spectrum [1]. Herschel's efforts in 1800 resulted in the development of the earliest detectors of heat radiation, such as Golay cells, bolometers, and thermopiles. For more than a century, all of the infrared detectors invented operated on the principle that incident radiation changed the temperature of the device and as a result, some temperature-dependent property could be measured to quantify the magnitude of the incident radiation [2]. The advantage of such thermal detectors is that they operate at ambient temperatures and consist of inexpensive materials. However, they also tend to be relatively insensitive and slow to respond. The drawbacks inherent to these devices stimulated research efforts in finding an alternate approach, which resulted in the proliferation of photon detectors.

Photon detectors are thin film semiconductor devices that undergo a change in free carrier density, i.e. conductivity, when exposed to incoming radiation. In these devices, photons with an energy greater than the forbidden energy gap of the semiconductor are absorbed, producing an electron-hole pair, thereby changing the amount of current flowing through the device. The output signal of the detector circuit is either a change in detector current or a change in voltage developed across a load resistor. In order to respond to IR photons, which have lower energies than photons in the visible range, the detector material needs to have a narrow bandgap [3]. Materials with narrow band gaps have a large conductivity at ambient temperature due to the thermal excitation of electrons and holes into the conduction and valance bands. This large conductivity at ambient

temperatures results in a noisy background signal, which can be suppressed by reducing the temperature. At the limit of 0 K, there are no thermal excitations, meaning no background signal. Cooling infrared detectors is generally regarded as the best method to enhance their overall performance.

Infrared sensors are used in a variety of applications, from gas and moisture analysers to human body detection to spectrophotometers. The wavelengths of interest for most applications are in the range of 3-5 μm and 8-12 μm [4]. The principal applications of infrared photon detectors have been military, which is drawn to the ability of these devices to detect and track hot or warm-bodied objects from far away and to provide passive night vision, as well as assistive daytime vision when smoke or mist limit visibility. The first photon detectors, made of thallus sulphide, were developed by the United States in World War I. Germany followed not long after, in the years leading up to World War II, with the next important development in this field with work on polycrystalline narrow-gap lead chalcogenide (PbS, PbSe, PbTe) thin films that extended the wavelength response further into the desired range of 3-5 μm [1,2]. There have been many developments in infrared photon detectors since this time, focused on the development of more complex alloys or doped photoconductors that make it possible to access higher wavelength ranges and/or produce more sensitive devices. While these new materials have led to the development of detectors that are very sensitive and fast, there are significant barriers for some applications: not only are they expensive, but these detectors also require cooling to cryogenic temperatures, particularly to detect longer wavelengths [4].

Lead sulfide (PbS) and lead selenide (PbSe) detectors are direct narrow band gap (0.28 eV) materials that have shown promise for relatively inexpensive IR sensing with modest cooling requirements. Chemically deposited lead selenide detectors have demonstrated excellent

detectivities in the 1-4.8 μm range even when operated at room temperature [5]. Intrinsic, or undoped, photoconductor detectors function well without significant cooling due to their longer excess-carrier lifetimes [6]. Lead chalcogenides crystallize in the cubic NaCl lattice structure and form complete solid solutions [7]. Alloy compositions can be varied to provide a very wide range of accessible energy gaps. Although lead chalcogenide sensors continue to be mass-produced and present a cost-effective option, they are only suitable for infrared detector applications in which limited sensitivity is not an issue. Limitations are also imposed on the scalability of lead chalcogenide by the standard fabrication process based on a chemical bath deposition technique (CBD) originally developed in 1965 [8, 9, 10]. As a result, lead chalcogenide detectors are predominantly only used in single-element detectors and small linear arrays [11].

The crystal quality of photon detector materials, which plays such a crucial role in their optoelectronic performance, is heavily dependent on the way the thin film device is manufactured. Device applications require very high quality alloys. Ideally, these materials have a homogeneity of composition, an absence of precipitation cracks, voids, and inclusions, low-angle boundaries, and a minimal number of dislocations [12]. Electrical properties, like carrier mobility, responsivity, and excess carrier lifetime are affected by the purity, deviation from stoichiometry, and degree of compensation [13]. Currently, thin films for high-performance IR applications, like those made out of HgCdTe (MCT), are made by molecular beam epitaxy (MBE). This technique along with others, like pulsed laser deposition (PLD), have been adapted to PbSe but are very slow and expensive processes [14, 15]. Other important methods include vapor, melt and vapor-liquid-solid (VLS) techniques. Growth from the vapor is attractive for a number of reasons [7]:

1. Vapor-grown crystals have lower concentrations of impurities due to lower growth temperatures and minimal contact with surfaces other than the substrate.

2. Precise control of supersaturation can be achieved by varying the growth conditions.

3. It is possible to regulate the deviation from stoichiometry.

4. Growth apparatus are simpler than for other techniques and therefore more economical.

In this study, we will grow lead chalcogenide thin films by vapor-liquid-solid (VLS) growth, which combines the advantages of thin film growth by vapor and liquid methods. VLS growth has primarily been used for growing nanowires. [15] Recent research from the Javey group at UC-Berkeley demonstrated that VLS growth can be applied to grow high-quality, polycrystalline thin films [16]. They were able to obtain indium phosphide (InP) thin films with large grain sizes and excellent optoelectronic properties by reacting a thin film of molten indium with phosphorous-rich gas. We are interested in leveraging the advantages of VLS growth to grow lead chalcogenide thin films. Grain boundaries hinder the speed of carriers in lead chalcogenide thin films to a few hundred Hertz for the most sensitized layers [4], so we are interested in both large grain size and attaining epitaxial growth.

# 2 Objectives

The goal of this project is to produce polycrystalline, epitaxial lead chalcogenide thin films with large grain sizes via vapour-liquid-solid (VLS) growth for applications in infrared sensing. We will begin by using PbSe as our system of interest. Should it result in successful growth and adequate optoelectronic performance, the technique can be expanded to PbS and Pb(S,Se) alloys. We are interested in understanding how growth conditions and sample preparation affect the thin film composition, morphology, and crystallographic texture. We will use glancing incident X-ray diffraction (GIXD), scanning electron microscopy (SEM), and 2D coupled X-ray scans (GADDS), respectively, to characterize these properties. Once we are able to achieve single-phase, continuous lead chalcogenide films, we will characterize the optoelectronic properties of the film with Hall effect and responsivity measurements. Since grain boundaries have been shown to impede optoelectronic performance of thin film materials, we want to grow polycrystalline films with large grains that are epitaxially matched with the substrate. The furnace system that we are using has the advantage of allowing us to tune many parameters of the growth process, including the partial pressure of the reactant, the total pressure of the system, the temperature and temperature ramp rate, and the composition of the reactant gas (i.e. can flow multiple gases at once).

# 3 Materials and Methods

## 3.1 Material selection

As there is eventual interest in growing an epitaxial lead chalcogenide thin film, growth substrates were selected with this specification in mind. Previous studies have demonstrated that high-quality epitaxial lead chalcogenide films can be obtained on (111)-oriented cleavages planes of $BaF_2$ substrates [4]. This fact is rather surprising given the lattice mismatch between the fluorite structure of $BaF_2$ (6.20 Å) and the rock-salt structure of PbS (5.94 Å) and PbSe (6.12 Å) is considerable, and the fact that vapour-grown IV-VI layers tend to grow in {100} rather than {111} orientations. $BaF_2$ substrates cleaved along the (111) plane were obtained from University Wafer. The size of the substrate was 10 cm by 10 cm. Lead shot (purity: 99.99%) was obtained from Sigma-Aldrich.

The choice to grow PbSe (rather than PbS) arose out of convenience, as the tube being used in the furnace was already contaminated with selenium. In the first growth experiment, our intent was to grow PbS. To our surprise, the experiment resulted in pure PbSe films even though we had flowed $H_2S$ gas. Some selenium deposits had remained in the furnace from a previous experiment and the reaction was favourable enough that PbSe formed preferentially over PbS. The eventual goal is to grow both PbS and PbSe, as well as alloys of the two Pb(S,Se).

## 3.2 Lead thin film deposition

Thermal evaporation was carried out in the "Organics Evaporator" in the Center for Materials Science and Engineering at MIT. The process involves heating a solid source material inside a vacuum chamber to the point at which the vapour pressure is high enough for the solid to

vaporize. This vapour travels across the chamber and deposits the material onto the substrate, resulting in a relatively uniform thin film. The lead thin film was deposited at a rate of 1 Å/s to make the thinner samples and a rate of 12 Å/s for thicker samples.

To maintain a sterile enclosure, the outer chamber was purged three times before anything was removed or inserted into the glovebox of the thermal evaporator. Tweezers were used to handle substrates. Direct contact with gloves or other surfaces was avoided to prevent contamination. The barium fluoride wafers were kept wrapped in wax paper and within a polyethylene storage container until they were removed within the glovebox. Because the sample holder was slightly larger than the substrates, the barium fluoride were placed at a 45° angle to prevent the substrate from falling through the cavity during the evaporation process. The substrates were attached at the corners, using as little surface area as possible. This sample holder was placed face down into the evaporation chamber. The chamber was then pumped down under vacuum for about 50-60 minutes.

Lead shot was loaded into a resistive evaporation filament, known as a "boat," which is essentially a thin sheet metal piece of suitable high-temperature metal (such as tungsten) with formed indentations or troughs into which the material is placed. Boat #2 was used in all experiments. Particle filtration masks, in addition to standard PPE, were donned for the duration of this step. Film thickness was monitored *in situ* by a quartz crystal monitor. Because the monitor cannot be in the exact same position as the sample being coated, there is a "tooling factor," which corrects the thickness data depending on how close the substrate is to the monitor. The tooling factor calculation is verified and confirmed by measuring the amount of material deposited on some samples and comparing it to the thickness the monitor measured. The tooling factor is calculated with the following expression:

$$F_m = F_i \frac{T_m}{T_i} \qquad (1)$$

where $F_i$ is the initial tooling factor, $T_i$ is the film thickness indicated by the instrument, and $T_m$ is the actual, independently measured thickness of the deposited film. The tooling factor $F_m$ used for subsequent thermal evaporation was 0.60.

## 3.3 Profilometry

Film thickness was measured using a Bruker Dektak XT stylus profilometer with a diamond tip. The thickness was quantified using Vision64 Data Analysis software. A scratch was made into the film surface with a razor and the profilometer readout was used to read the difference between the bottom of the scratch and the surrounding material. Several scratches were made on each sample in different locations to obtain a representative measurement. These initial thickness measurements were used to adjust the tooling factor for future thermal evaporations.

## 3.4 Lead selenide growth

Lead selenide (PbSe) was grown in a 3-zone tube furnace with $H_2Se$ as the reactant. The growth regime is illustrated in Figure 1. We chose a growth temperature of 350°C, because it is above the melting point of lead. The 20-min growth duration was taken from the Javey Group protocol [15]. Samples were first heated under vacuum to a temperature of 300°C at a ramp rate of about 5°C/min. The temperature was then ramped up to 350°C at the same rate. As the temperature passed the melting point of lead (327°C), the flow of $H_2Se$ was activated at a flow rate

of 75 SCCM. Once the thermocouple read out a temperature of 350°C, the growth was run for 20 minutes, after which the gas flow was shut off and the set point was lowered to room temperature. After the furnace had cooled to a slightly lower temperature, we initiated the purge routine. In the next 1.5-2 hours, the temperature fell to ~80°C and we removed the sample from the furnace.

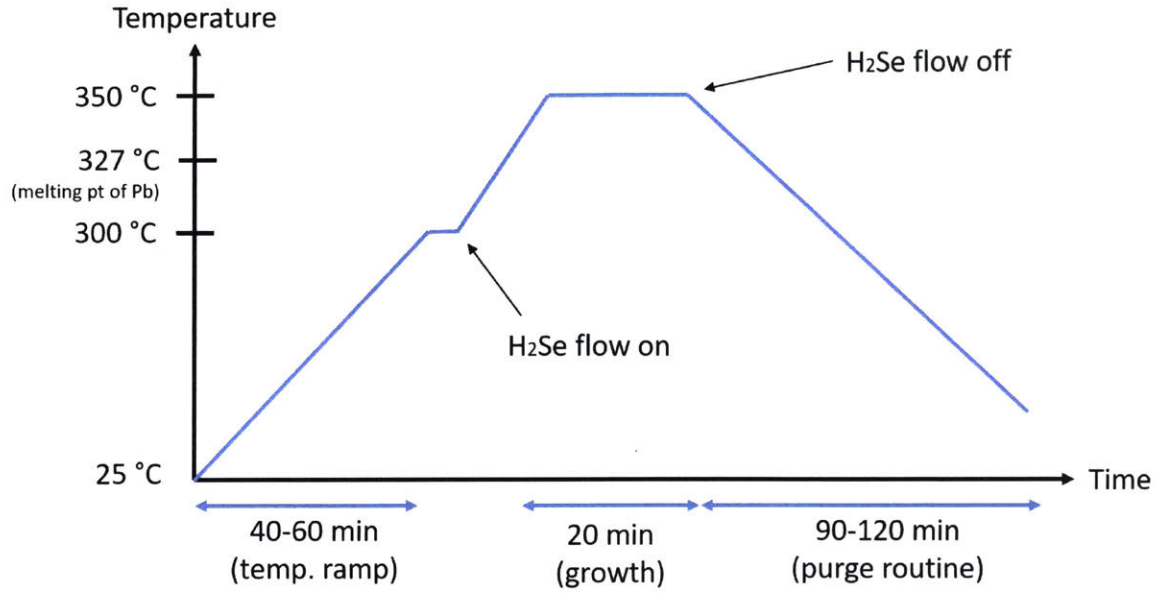


*Figure 1. Temperature profile during growth experiments (not to scale).*

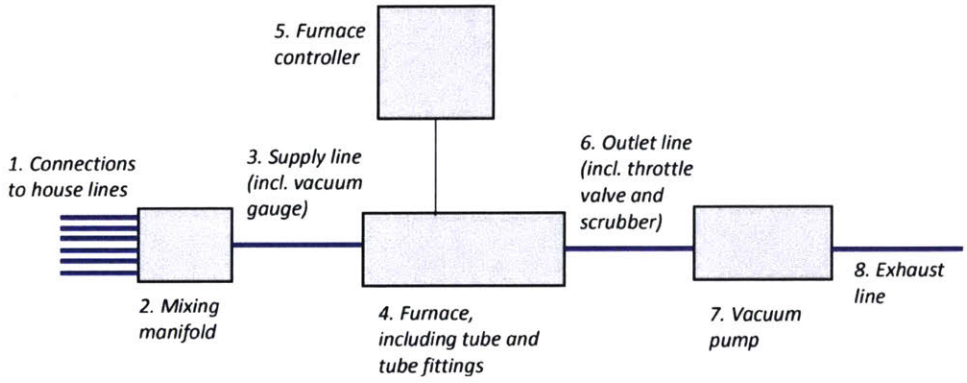


*Figure 2. Schematic of furnace setup.*

The temperature in Region 2 of the tube furnace was actively controlled, while the temperatures in Regions 1 and 3 were not regulated. These zones generally reached temperatures of about 250°C during the growth stage. This may have had the consequence of volatilizing any solids that happened to be present on the ends of the tube furnace, although composition analyses of the samples post-growth did not indicate significant concentrations of impurities.

## 3.5 X-ray diffraction analysis

X-ray diffraction analyses were conducted on a Rigaku SmartLab using grazing incidence X-ray diffraction (GIXD). The instrument features a 9kW rotating anode copper X-ray source. Measurements were performed using a parallel beam (PB) optics alignment with a parallel slit analyser (0.114 PSA). The Parallel-Beam (PB) geometry uses a Gobel mirror to focus the divergent X-ray beam into a nearly parallel X-ray beam, which allows the incident angle and the diffraction angle to be decoupled during the scan. GIXD allows the X-ray beam to be focuses in the surface of the sample, increasing the amount of signal that comes from the thin film or sample surface. A 5-mm IS-L slit, which is used to match the length of the X-ray beam to the height or our sample, was used for optics alignment (the IS-L slit should be at least 20% smaller than the sample). After the alignment, the slit was changed to a 10-mm slit to allow for maximum intensity to fall on the sample during the scan. A continuous scan was done from a $2\theta$ angle of 20° to 90° at increments of 0.02° and a speed of 4°/min. The glancing incident angle was 1°.

The resulting spectra were analysed using the High Score Plus v3.0 software to determine the sample composition. Scherrer analysis, via Williamson-Hall plots, was conducted to determine the average crystallite size and microstrain. Lanthanide hexaboron ($LaB_6$) was used as the nanocrystalline standard for the Scherrer analysis.

## 3.6 Scanning electron microscopy

The morphology of the thin films was inspected using the Zeiss Merlin scanning electron microscope (SEM), which is capable of high resolution secondary electron imaging with a resolution of 0.8 nm at 15 kV and 1.4 nm at 1 kV with an in-lens secondary electron detector. Samples were imaged as-grown at several magnifications.

## 3.7 Crystallographic texture analysis

We analysed the orientation of crystallographic planes in the samples using the Bruker D8 General Area Diffraction Detection System (GADDS). The GADDS has a two-dimensional area detector, which captures more of the diffracted X-rays and facilitates the evaluation of texturing in the sample. This system uses a conventional 1.6kW sealed tube copper anode. Our 2D coupled scan consisted of 4 frames, 15° per frame, and 600 seconds per frame. Separate pole figure analyses were conducted to generate a stereographic projection of crystals in the sample. We used DIFFRAC.EVA software to analyse the coupled scan data and Multex Area 2 to analyse the pole figure data.

# 4 Results & Analysis

## 4.1 Overview

Throughout these experiments, crystal quality was evaluated by the average crystallite size and microstrain. The subsections discuss the variables that were manipulated in an attempt to improve crystal quality and attain epitaxial growth. A summary of the samples grown in these experiments is summarized below (Table 1).

*Table 1. Summary of samples grown. Variables changed relative to the previous samples are highlighted in yellow.*

| Sample designation | Experimental sample name | Substrate | Film thickness | Growth temp | Final film composition | Capping layer? |
|---|---|---|---|---|---|---|
| Sample A | PbSe_030818 | $SiO_2$ | 300-400 | 350 | PbSe | No |
| Sample B | PbSe_031018 | $BaF_2$ | 300-400 | 350 | PbSe | No |
| Sample C | PbSe_032618 | $BaF_2$ | 60-100 | 350 | PbSe, $BaSe_3$ | No |
| Sample D | PbSe_032718 | $BaF_2$ | 60-100 | 250 | PbSe, $BaSe_3$ | No |
| Sample E | PbSe_041718 | $BaF_2$ | 60-100 | 350 | PbSe, $BaSe_3$ | Yes |
| Sample F | PbSe_041818 | $BaF_2$ | 60-100 | 250 | PbSe, $BaSe_3$ | Yes |

## 4.2 Effect of substrate ($SiO_2$ vs. $BaF_2$)

As discussed in the Introduction, previous research efforts demonstrate that high-quality epitaxial thin films of lead chalcogenides can be obtained on (111) $BaF_2$ substrates. Our first growth experiment focused on evaluating the effect of substrate on PbSe crystal quality. Growth conditions were the same for the two substrates: an approximately 150 nm thin film of lead was exposed to 75 SCCM of $H_2Se$ at 350 °C for 20 minutes. Due to its cubic nature and one-to-one stoichiometry, it is estimated that the resulting PbSe film, if grown successfully would approximately double in thickness. Analysis of GIXD measurements revealed that single-phase PbSe was obtained on both $BaF_2$ (Fig. 3a) and $SiO_2$ (Fig. 3b) substrates. SEM images reveal similar

thin film morphology, in which small polycrystalline samples form a relatively uniform layer that appears to be slightly porous. Visual inspection of the SEM image (Fig. 4) suggests that there is no epitaxy present on the top surface, and texture analysis conducted using a 2D coupled X-ray scan (GADDS) corroborates this observation.

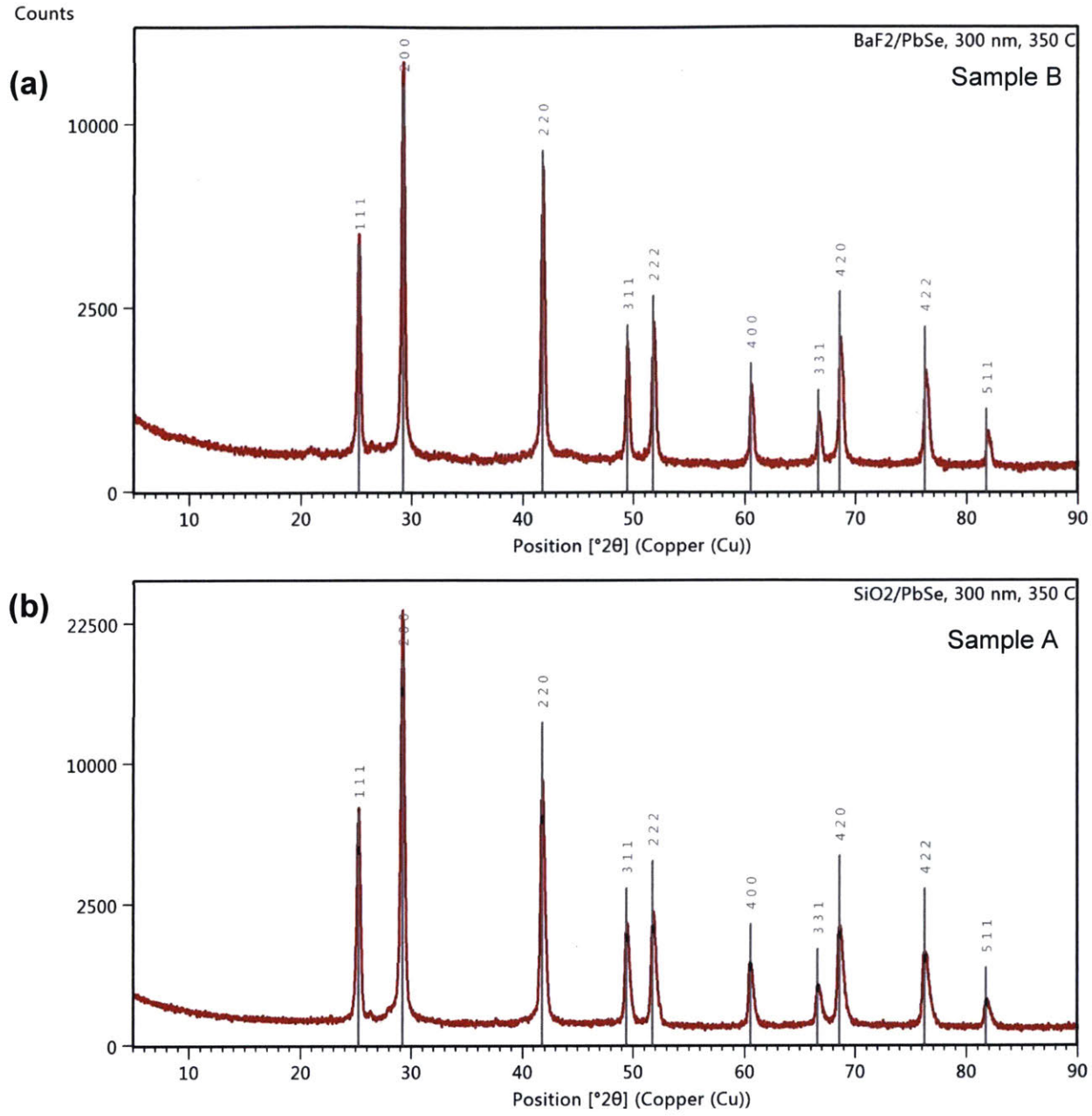


*Figure 3. GIXD spectrum of PbSe grown by vapor-liquid-solid growth on (a) $BaF_2$ substrate [Sample B] and (b) $SiO_2$ substrate [Sample A] at 350 C for 20 minutes under $H_2Se$ (flow rate of 75 SCCM). Measurements taken at a 1° glancing angle. Profile shows single-phase PbSe thin film achieved.*

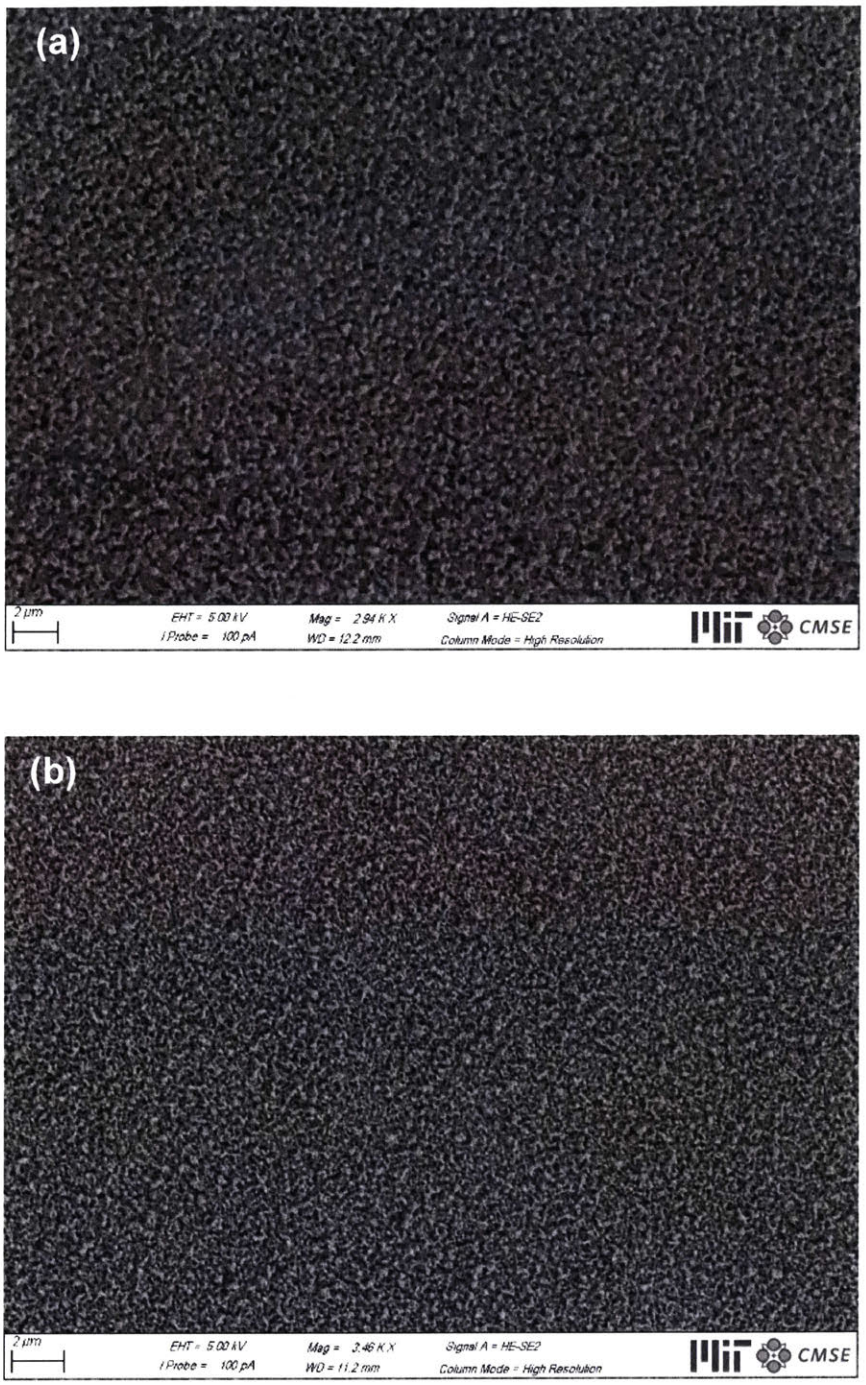


*Figure 4. Scanning electron microscope (SEM) image of PbSe thin film (approx. 300-400 nm) on (a) $BaF_2$ substrate [Sample B] and (b) $SiO_2$ substrate [Sample A] grown using vapour-liquid-solid (VLS) method.*

Williamson-Hall analysis was conducted on the profiles of both samples to calculate the average crystallite size and the microstrain present in the crystal structure. This analysis is based on the Scherrer equation, which relates the measured diffraction angle to the shape of the resulting peak.

$$\Delta 2\theta = \frac{k\lambda}{L\cos\theta} + 4\varepsilon\frac{\sin\theta}{\cos\theta} \qquad (2)$$

where $\theta$ is half of the Bragg angle of diffraction, $\Delta 2\theta$ is the peak width at full width half maximum (FWHM), $\lambda$ is the wavelength of X-ray source (for Cu, $\lambda = 1.54$ Å), k is the shape factor (we approximate spherical particles, so k = 0.9), L is the crystallite size, and $\varepsilon$ is the microstrain that results from lattice distortion.

The equation above can be put into the standard form of a linear equation, $y = mx + b$, where m is the slope and b is the y-intercept. In transformed equation below (Equation 3), the slope would be $\varepsilon$ (representative of the % microstrain) and the y-intercept is $\frac{k\lambda}{L}$ (representative of the average crystallite size).

$$\Delta 2\theta\cos\theta = \frac{k\lambda}{L} + 4\varepsilon\sin\theta \qquad (3)$$

Fig. 5 displays the same Williamson-Hall plots for Samples A and B, with the best-fit line taking into account the contributions from both microstrain and average crystallite size.

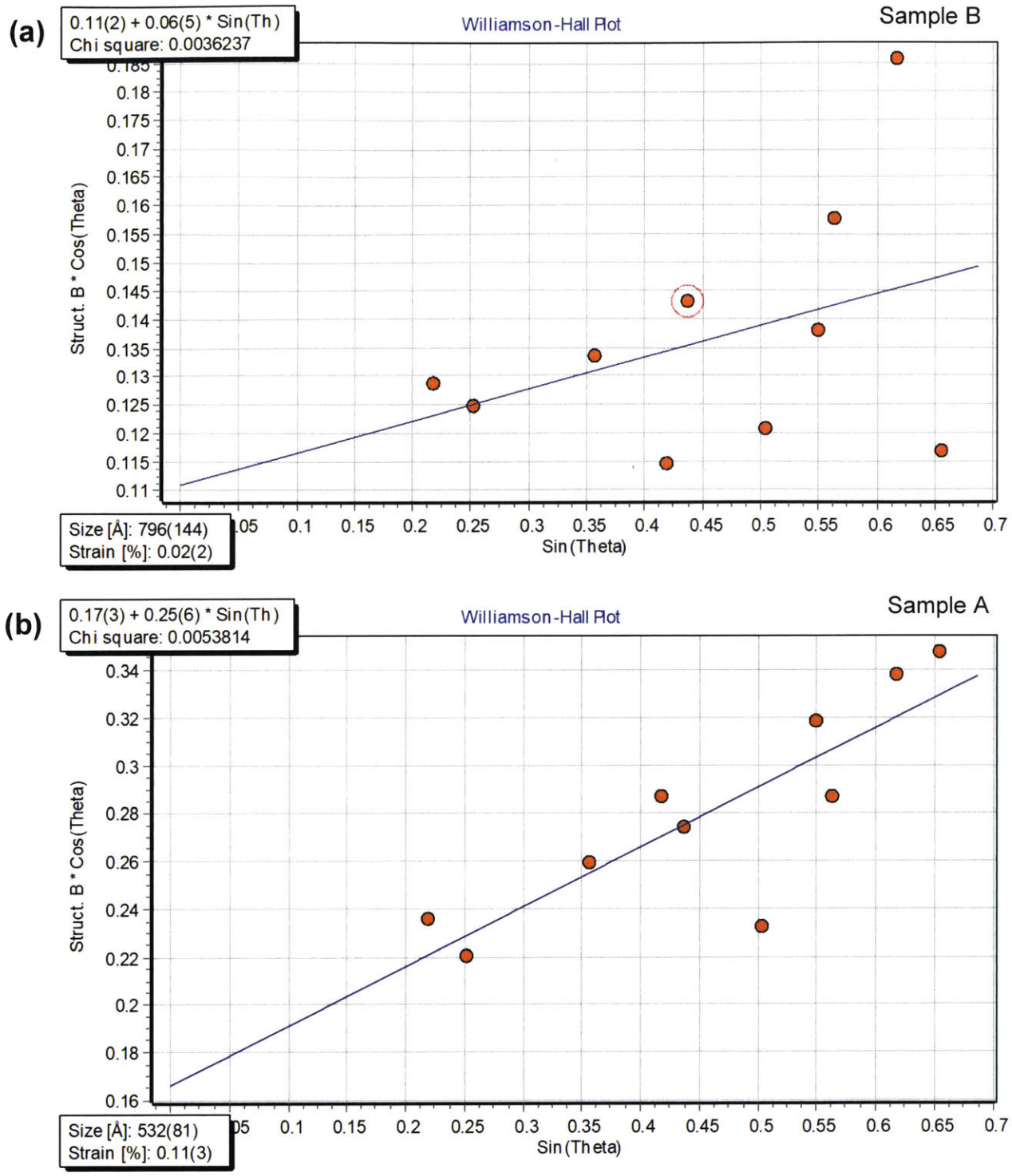


*Figure 5. Williamson-Hall plots of PbSe grown on (a) $BaF_2$ substrate [Sample B] and (b) SiO2 substrate [Sample A]. The values for the microstrain and the average crystallite size are displayed for each plot on the bottom left. The equation on the top left is the fit to the Cagliotti equation.*

The values for average crystallite size and microstrain determined by Williamson-Hall and Scherrer analyses are summarized in Table 2 in section 4.6. A comparison of the crystal quality of the PbSe films achieved from two different substrates, silicon oxide and barium fluoride, reveals that the substrate on which the thin film is grown makes a difference, even though the layers are not epitaxial. The more closely lattice-matched $BaF_2$ substrate results in larger crystallites on average (79.6 nm vs. 53.2 nm) and slightly less lattice distortion (microstrain: 2% vs. 11%).

## 4.3 Effect of film thickness

The fact that we were able to obtain a single-phase PbSe film, which wasn't at all a certainty before we began experimentation, suggested that the growth conditions used in the first experiment were an adequate starting point for subsequent experiments. Rather than tuning the growth parameters (e.g. flow rate, temperature ramp rate, duration of growth), we decided that one way of moving closer towards achieving epitaxial growth would be to grow PbSe from thinner films, in order to increase the importance of the film-substrate interaction. For the third growth experiment, designated Sample C, instead of depositing a 150-200 nm layer of lead onto the substrate, we deposited 30-50 nm. Growth conditions were otherwise the same as for Samples A and B.

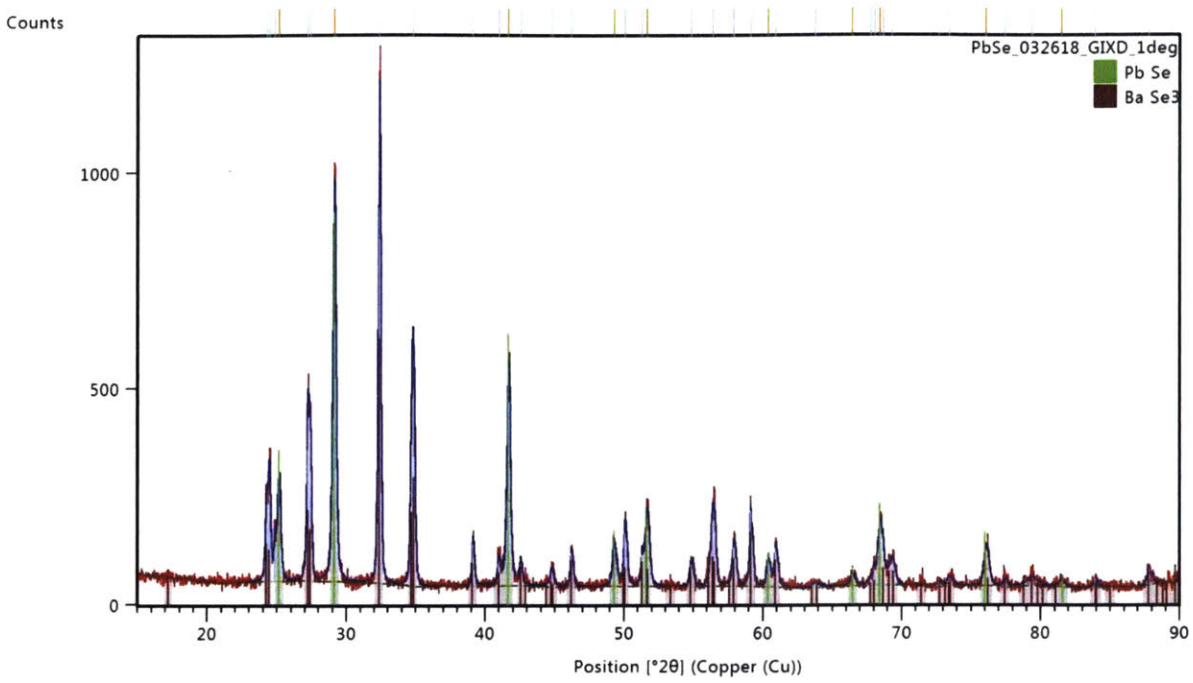


*Figure 6. GIXD spectrum shows presence of PbSe and $BaSe_3$ in Sample C. Measurements taken with a 1° glancing angle.*

The XRD results for Sample C (Fig. 6-7) show that instead of having single-phase PbSe in our film, there are in fact two phases present. The spectrum has the fingerprints of both PbSe and $BaSe_3$. These findings suggest that the $H_2Se$ gas had reacted not only with the molten lead but also with the solid $BaF_2$ substrate underneath the lead thin film. Closer inspection with scanning electron microscopy (Fig. 8) shows two regions of different color, which suggests that both the PbSe and the $BaSe_3$ phases are present on the surface of the sample, rather than having one forming on top of the other. From this evidence, it is not immediately clear why the two phases are forming, but there seem to be two possible explanations. One is that as the lead film becomes thinner, it is more prone to dewetting. As the lead film dewets, it uncovers the underlying $BaF_2$ substrate, thus allowing it to react with the incident $H_2Se$ and form $BaSe_3$. Another explanation is that the diffusion kinetics involved in the reaction that forms $BaSe_3$ are rapid and because the lead film is thinner, the selenium atoms diffuse quickly through this surface layer and reach the substrate, with which they react.

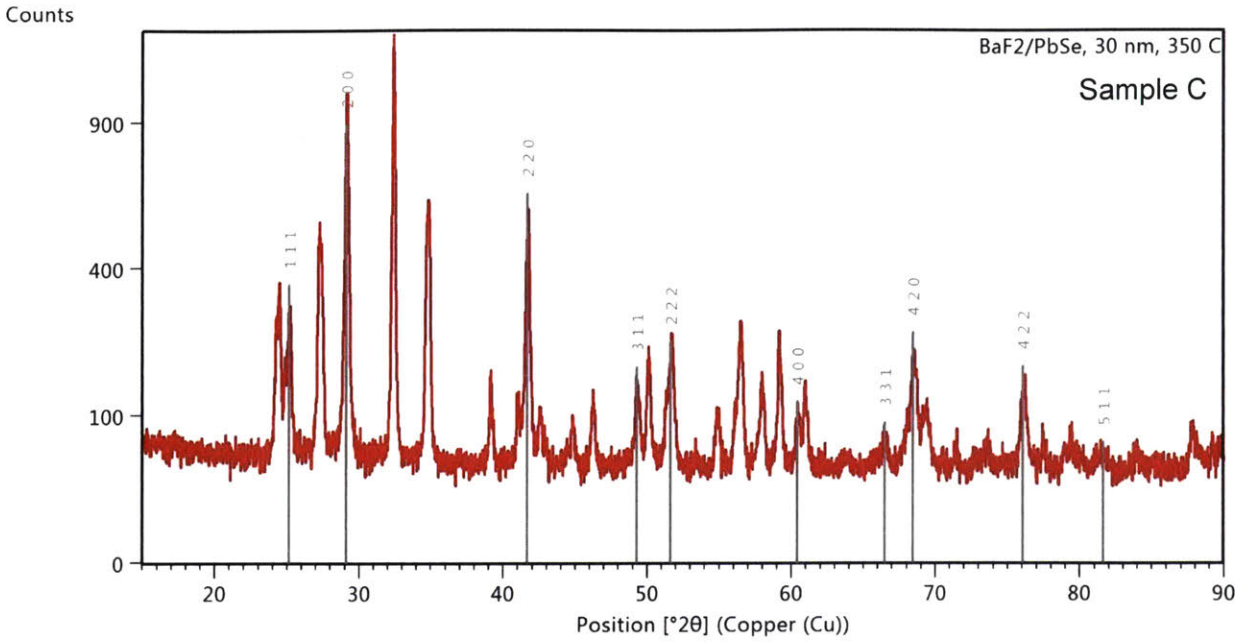


*Figure 7. GIXD spectrum of Sample C shows presence of PbSe and $BaSe_3$ on sample surface. Measurements taken with a 1° glancing angle. PbSe peaks are labelled with relevant Miller indices. The unlabelled peaks correspond to those of $BaSe_3$.*

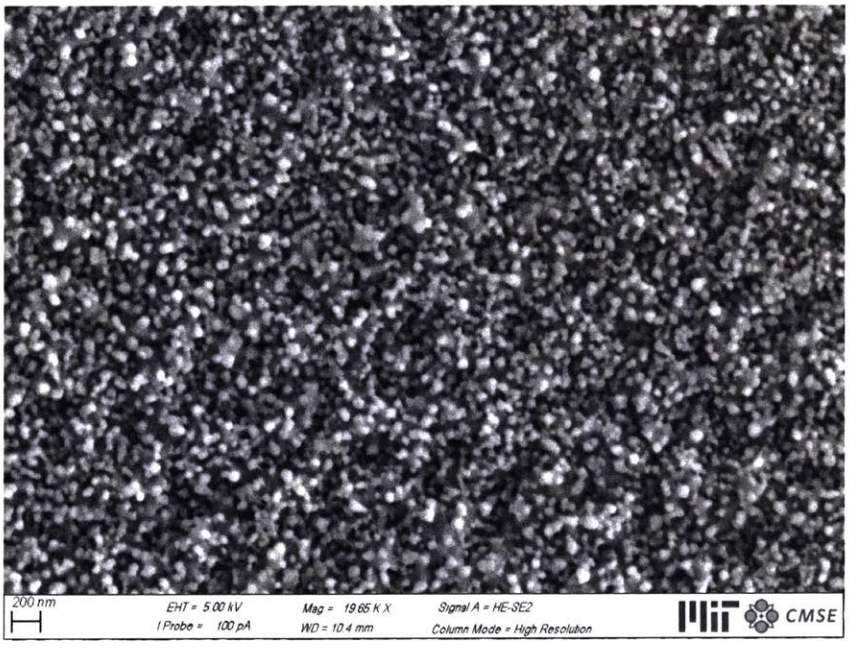


*Figure 8. SEM image of Sample C, which underwent VLS growth at 350°C. Mottled coloration of surface is interpreted as intermingling of two distinct compositions: PbSe and $BaSe_3$.*

Because there are two phases present in this sample, it makes it more difficult to calculate average crystallite size and microstrain using the Williamson-Hall plot. As can be seen in Figure 9, some of the data points are assigned a default value of zero, which skews the slope and y-intercept of the plot. The orange points are those associated with PbSe profile peaks and the light blue points result from the $BaSe_3$. Even if the latter are excluded from the calculation, the result is clearly not accurate (e.g. the average crystallite size is negative). This is because some of the BaSe3 peaks overlap with PbSe peaks, which affects the breadth and width of the given peak. Since the full width half max (FWHM) of the peak is involved in the Scherrer analysis, including overlapping peaks into the calculation skews the final values.

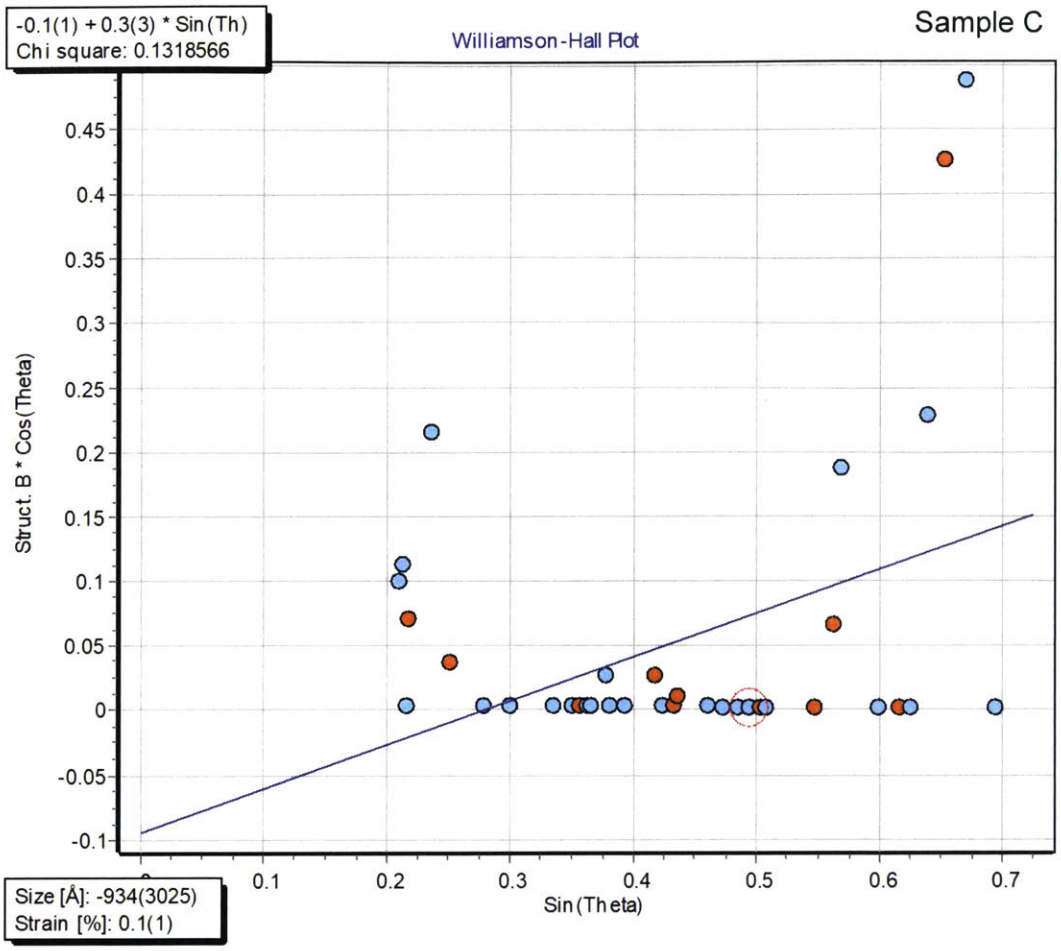


*Figure 9. Williamson-Hall plot of Sample C, which contains PbSe and $BaSe_3$ regions. The distribution of the points and the negative value for crystallite size indicate that performing Scherrer analysis on the whole profile is not appropriate. Orange points correspond to PbSe peaks and light blue points correspond to $BaSe_3$ peaks.*

The complications involved in performing Scherrer analysis on samples with more than one prominent phase can be resolved by basing the calculation on an independent PbSe peak (one whose FWHM is not influenced by proximity to a $BaSe_3$ peak). An important source of line broadening in polycrystalline materials is finite crystal size. Most crystals are composed of a mosaic of blocks that are slightly misaligned relative to one another. Crystallites smaller than 120nm in diameter cause broadening of diffraction peaks (instrument specific). In crystals of finite dimensions, there is incomplete destructive interference of waves scattered from angles slightly deviating from the Bragg angle. If we define the angular width of a peak at half height as

$$B = \frac{1}{2}(2\theta_1 - 2\theta_2) \qquad (4)$$

then, the average crystallite size, L, can be estimated from the first term of the Scherrer formula (equation 2), which corresponds to the crystallite size contribution:

$$L = \frac{0.9\lambda}{B\cos\theta_B} \qquad (5)$$

Where $\theta_B$ is Bragg's angle and B is peak width (FWHM) expressed in radians, and $\lambda$ is the wavelength of the X-ray source (in this case, copper). Microstrains also give rise to peak broadening via a variation of the interplanar spacing and hence diffraction occurs over a range of 2θ angles. The contribution of the microstrains in peak broadening is given by:

$$B = \varepsilon \tan\theta_B \qquad (6)$$

where $\varepsilon$ depends on the strain distribution. A summary of the calculations derived from Scherrer analysis are presented in Table 2 in Section 4.6.

## 4.4 Effect of growth temperature

To understand how vapour-liquid-solid (VLS) growth affects PbSe crystal quality in comparison to growth from a solid thin film that is exposed to a gaseous reactant, we grew films at two different growth temperatures. Samples grown at a final temperature of 250°C constituted growth from the solid phase, while those grown above the melting point of lead (327°C) at 350°C (Samples A-C and E) constituted VLS growth. At 350°C, the $H_2Se$ gas would be flowing over a molten film of lead.

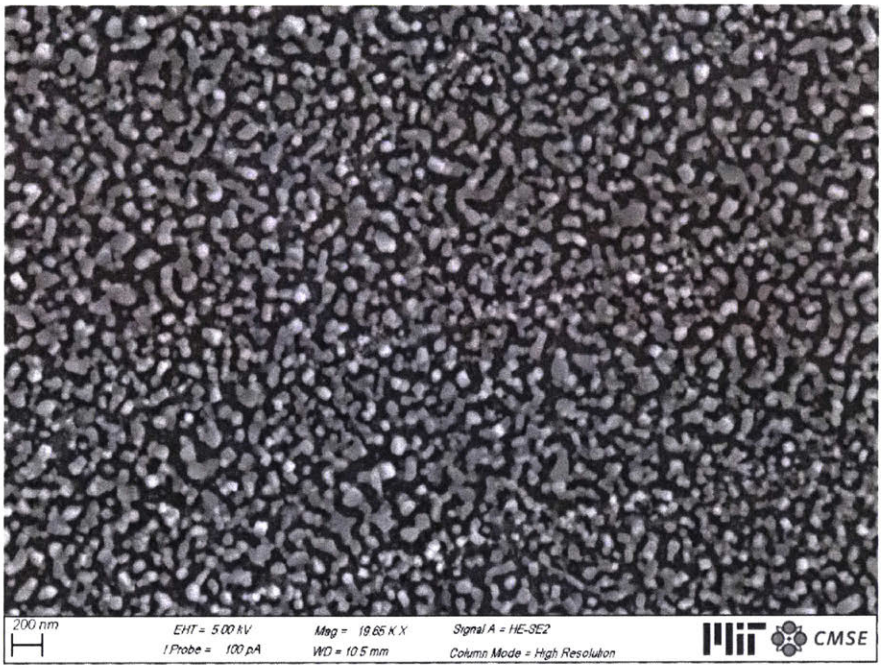


*Figure 10. Scanning electron microscope (SEM) image of Sample D suggests dewetting is occurring in thinner Pb films during annealing. The lighter regions are the PbSe phase, while the darker regions are $BaSe_3$ and $BaF_2$.*

The SEM image of Sample D (Figure 10) shows evidence of dewetting in the thin film, which means that the thin film is rupturing and the lead is pooling together to form a discontinuous network of solid lead across the substrate. The morphology of the film suggests that the lead film is dewetting, exposing the $BaF_2$ substrate in the regions from which the lead film has receded.

Because the $H_2Se$ is in direct contact with these regions and it is a reactive compound, $BaSe_3$ is forming. For optoelectronic applications, this effect is undesirable.

## 4.5 Effect of capping layer

In their investigation on VLS growth of InP, the Javey Group addressed the issue of thin film dewetting by depositing a capping layer of amorphous silicon oxide on the surface of their pre-growth sample [15]. This capping layer serves two purposes. For one, it maintains the planar geometry of the thin film of interest. It also slows the diffusion of $H_2Se$ through the film, thereby preventing the reactive gas from reaching the substrate as quickly and possibly affecting the reaction kinetics of PbSe, which could have a significant effect on the crystal quality of the resulting film. We deposited a 50 nm layer of $SiO_2$ by electron beam deposition onto the thin lead films (30-50 nm), which we designate Sample E and F. The growth conditions were consistent with our earlier experiments. We investigated two different growth temperatures (250°C and 350°C) to continue to evaluate the effect of VLS growth on crystal quality and growth mode.

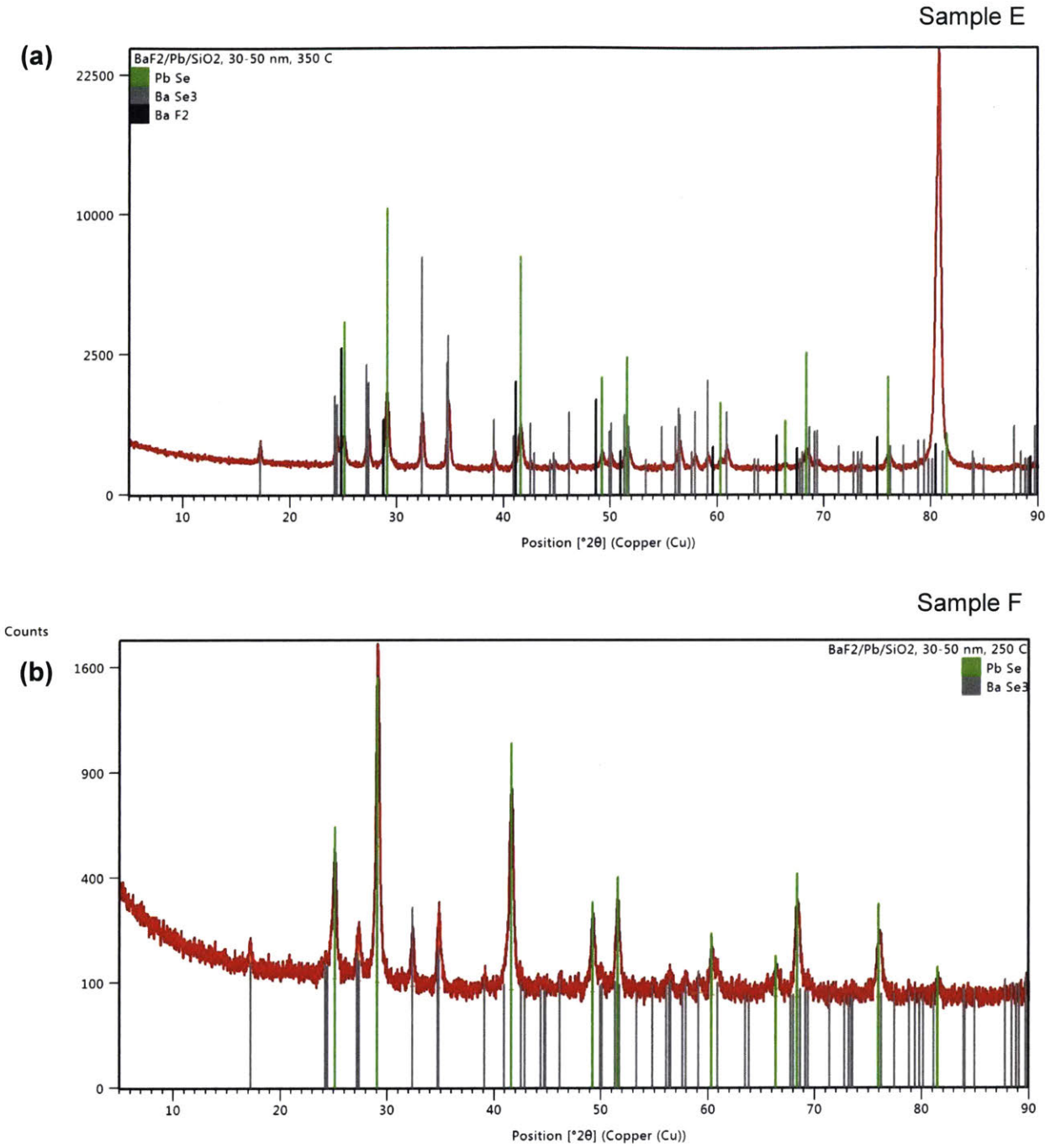


*Figure 11. XRD spectra for (a) Sample E and (b) Sample F, both covered with a 50 nm silicon oxide capping layer.*

A comparison of the XRD spectra (Fig. 11) allows one to observe the effect that the capping layer had in growth from the vapour to solid phase (250°C) and with VLS growth (350°C). Both samples contained PbSe and $BaSe_3$, but it is interesting to note that the sample that underwent VLS growth (Sample E) has a lower concentration of the undesirable $BaSe_3$ phase. Sample E also has a larger average PbSe crystallite size than Sample F (see Table 2 in Section 4.6), which may be a consequence of the higher growth temperature slowing down the nucleation rate. In the XRD profile for Sample E, the very large diffraction peak at a $2\theta$ of around 80° is due to diffraction from the (511) peak of the $BaF_2$ substrate.

Knowing more about the surface morphology of the thin film would shed more light on the mechanism by which this secondary phase is forming and the effect that modulating the diffusion rate via a capping layer has on the growth and nucleation within the liquid and solid film. In order to be able to image the surface of the thin film using SEM, it was necessary to remove the 50nm silicon oxide capping layer. The standard procedure for removing native or deposited silicon oxide layers is to etch the surface with a dilute HF solution. Using a 2% HF solution diluted in water, the capping layer was removed by immersion in the etchant for 7.15 minutes, after which it was rinsed with water and dried with nitrogen air. Although there was some concern that HF would etch PbSe or the $BaF_2$ substrate, the HF did not seem to affect the integrity of the lead selenide thin film. What was not foreseen is that the use of water as a diluent posed a significant problem, because $BaF_2$ substrate is soluble in water [4]. As this was learned by trial and error, these samples were compromised, because chunks of the thin film peeled off of the substrate. As a result, it was not possible to obtain quality SEM images of the PbSe layer. The SEM image below shows the $BaF_2$ surface that has been etched by water (Figure 12).

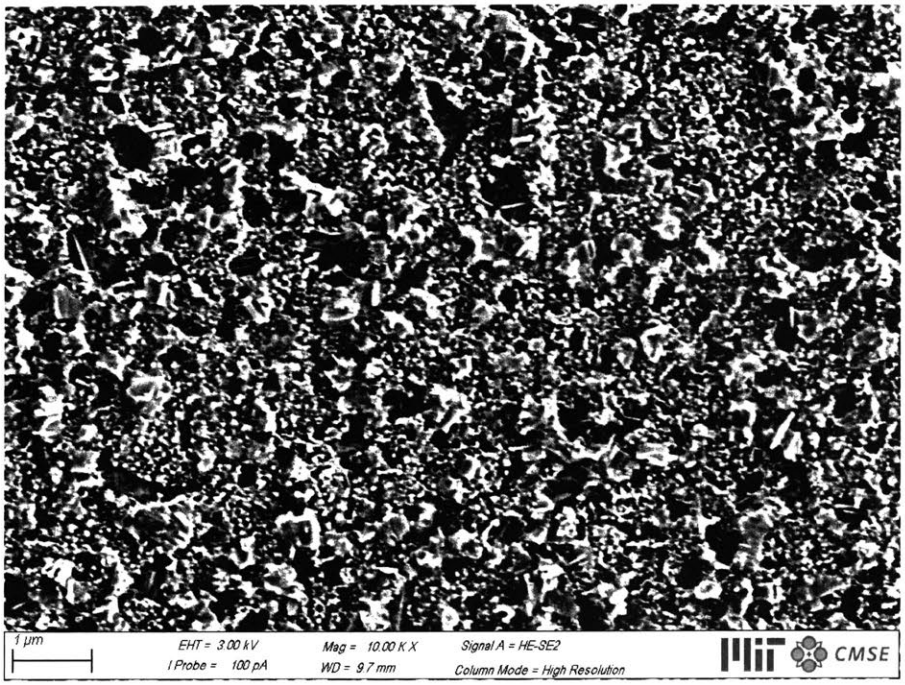


*Figure 12. SEM image of $BaF_2$ substrate etched with water. Samples E and F could not be imaged as a result.*

## 4.6 Overview of Scherrer analysis

Table 2 summarizes the results for the Scherrer analysis. Samples A and B were analyzed with Williamson-Hall plots. Samples C-F did not consist of a single phase like Samples A and B, so it was not appropriate to use Williamson-Hall calculations to report on the crystal quality for these samples. For Samples C-F, we calculated the average crystallite size and microstrain manually from the FWHM of the (200) PbSe peak using the Scherrer formula. The (200) peak was chosen because it did not overlap with any of the substrate peaks or the $BaSe_3$ peaks, so the FWHM of the peak was only influenced by the PbSe phase. Sample D was not analysed with the Rigaku SmartLab instrument due to time constraints. While the manual, single-peak analysis can provide a reasonable estimate for the average crystallite size, it becomes much weaker for determining the microstrain contribution, so those values may be less accurate representations of the microstructure.

*Table 2. Summary of microstrain and average crystallite size values for various experiments*

| Sample name | Sample layers | Initial Pb thickness (nm) | Growth temp (°C) | Crystallite size contribution (Å) | Microstrain contribution (%) |
|---|---|---|---|---|---|
| **Sample A** | $SiO_2$/Pb | 300-400 | 350 | 532 | 0.11 |
| **Sample B** | $BaF_2$/Pb | 300-400 | 350 | 796 | 0.02 |
| **Sample C** | $BaF_2$/Pb | 60-100 | 350 | 309 | 0.01 |
| **Sample D** | $BaF_2$/Pb | 60-100 | 250 | - | - |
| **Sample E** | $BaF_2$/Pb/$SiO_2$ | 60-100 | 350 | 378 | 0.04 |
| **Sample F** | $BaF_2$/Pb/$SiO_2$ | 60-100 | 250 | 297 | 0.05 |

## 4.7 Analysis of thin film texture

In addition to understanding the evolution of crystal quality in these films, we are also interested in the effect of substrate, sample preparation, and growth conditions on the presence of preferential crystallographic orientation, or texturing, in the polycrystalline lead selenide films. We used a General Area Detector Diffraction System (GADDS) to determine whether any of the samples exhibited epitaxial growth or preferential crystallographic orientation, which would give us direct evidence of the growth mode. A 2D coupled scan allowed us to qualitatively analyse whether any epitaxy or texture was present in the thin film (Fig. 13). This analysis was conducted on Samples B and C, which varied in the thickness of the deposited lead. Unfortunately, we were only able to use the Bruker D8 GADDS system for a few measurements, because shortly after the data was collected, the instrument went into disrepair for several weeks.

The scan of Sample B (Fig. 13a) shows a truncated ring on the far right. This is the (111) peak in the PbSe profile, which occurs at a $2\theta$ of 25.15°. The fact that this peak only diffracts across a certain range of the scan indicates that there is a preferential crystallographic orientation in the film. Meanwhile, the scan of Sample C (Fig. 13b) does not reveal any inhomogeneity in the intensity of diffraction off of the (111) plane, but there appears to be some texturing in the fifth ring from the right, with the bands becoming more intense on the outer edges. We determined this to be the (210) peak of $BaSe_3$. Sample C was characterized further with out-of-plane pole figure analysis.

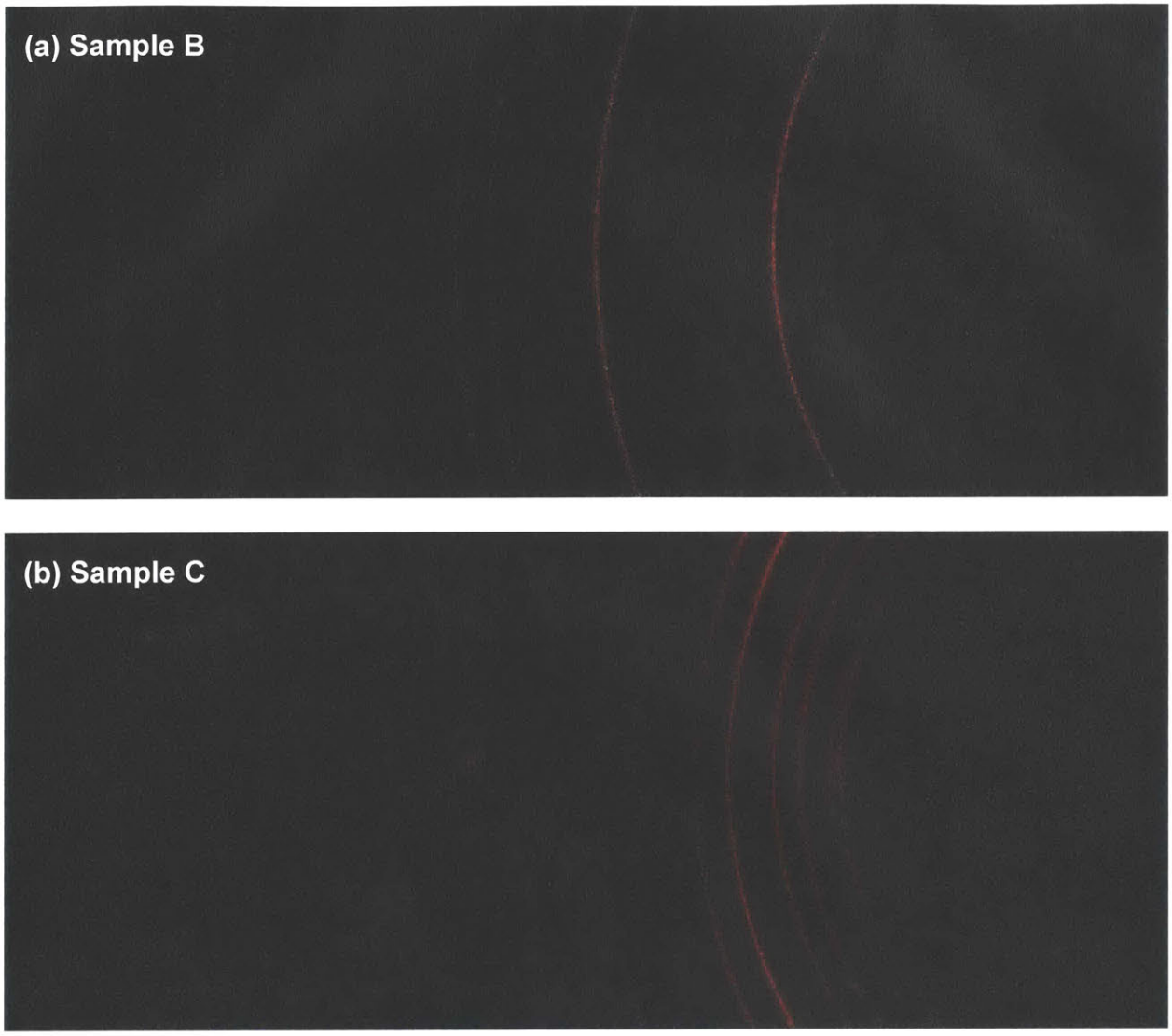


*Figure 13. Diffraction data from a 2D coupled scan taken on the Bruker D8 General Area Diffraction Detection System (GADDS) (a) Sample B: The truncated band of intensity suggests some preferential crystallographic orientation. (b) Sample C: The enhancement of band intensity in some areas may be indicative of texturing. The bright spot on the outer rings is likely a sharp signal from the single crystal $BaF_2$ substrate.*

To characterize the texturing more directly, we used an out-of-plane pole figure analysis (using the Bruker D8 GADDS system), which allows us to construct a stereographic projection of the sample that reveals the planes along which there is especially strong diffraction, thus indicating a preferred orientation in the film. The pole figure analysis revealed that the PbSe (Fig. 14a) is randomly oriented, i.e. not textured, while the $BaSe_3$ regions (Fig. 14b) had a preferred orientation along the (201) and (220) planes. It is unknown whether the PbSe regions do not display any texturing because PbSe is not prone to do so under these growth conditions or because the secondary $BaSe_3$ is disrupting any preferential growth mode that PbSe may have had.

Since we have such a thin film, the substrate outputs a disproportionately strong signal in out-of-plane measurements. The pattern that results in Figure 14a is noise that becomes more pronounced when we impose a threshold on the diffraction intensity so that the peak from the substrate doesn't overshadow everything else. We would recommend that for future experiments on these films, in-plane pole figure analysis on the Rigaku SmartLab be used for investigating crystallographic orientation.

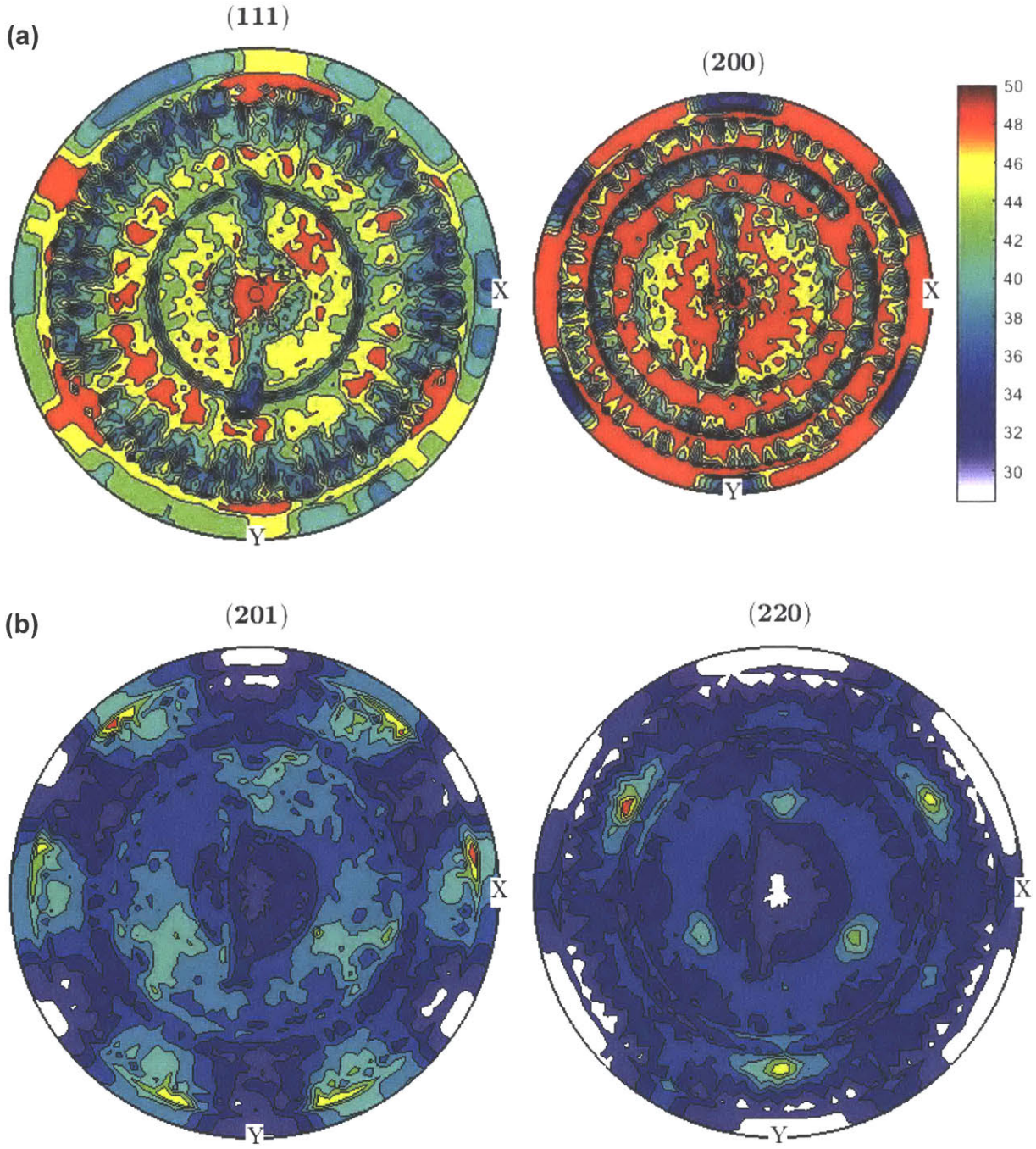


*Figure 14. Stereographic projection of crystal structure in Sample C (PbSe thin film (30-50 nm) with presence of $BaSe_3$). Grown under VLS growth conditions. The pole figure analysis reveals no texture in the PbSe (a) and preferential orientation in the (210) and (220) planes of $BaSe_3$ (b).*

# 5 Discussion

The Javey Group at Berkeley demonstrated that VLS growth, a technique traditionally used to grow nanowires, can be used to obtain high-quality polycrystalline thin film samples. They were able to expertly engineer the nucleation rates in their films to ensure large grain sizes of 10-100μm, by patterning the substrate with preferential nucleation centres, thereby triggering heterogeneous growth only at these foci. We were inspired by their work to try VLS growth as a means to achieve polycrystalline, epitaxial thin films of PbSe. This experiment has shed light on the properties and growth modes of PbSe thin films grown by this method. This initial foray into growing PbSe films has laid down some groundwork that will enable further work on this class of infrared photon detectors. We have not yet achieved especially large grain sizes or epitaxial growth in the PbSe thin films, but the results thus far point to the next experiments that can be done to improve the crystal quality and to relate the thin film characteristics to optoelectronic properties.

We have demonstrated that the choice of substrate has an effect on the average crystallite size and the microstrain present in the thin film. Substrate choice is an important consideration when one is trying to attain epitaxial films, but even if epitaxial growth is not present, the substrate-film interaction affects the growth mode and microstructure of the resulting material. In an attempt to increase the importance of the film-substrate interaction, we decreased the thickness of the film we were growing. The decrease in the thickness of the film resulted in the formation of a secondary $BaSe_3$ phase, in addition to the PbSe phase, indicating that the hydrogen sulphide gas was reacting with the substrate, either as a result of the lead film dewetting and exposing the substrate or due to the more rapid reaction kinetics between the substrate and gaseous reactant. We added a silicon oxide capping layer to slow down diffusion and prevent dewetting of the lead film. The capped sample grown by VLS growth (Sample E) had larger crystallites on average than either the

uncapped VLS growth (Sample C) or the capped non-VLS growth (Sample F), suggesting that the capping layer slows diffusion, and therefore nucleation rate, and that VLS growth results in larger crystallites, either due to the higher growth temperature or a growth mode that is inherent to VLS. This question needs to be explored in greater detail.

Through the use of vapour-liquid-solid (VLS) growth, our goal is to achieve heterogeneous nucleation and epitaxial primary grain growth. The appearance of $BaSe_3$ on the surface of the thinner samples (Samples C-F) and the observed particle sizes suggest that was is actually occurring is rapid homogeneous nucleation followed by primary grain growth in the solid thin film. These results suggest that we are over-selenizing our system. Nucleation rate is dependent on the concentration of the reactant. In the context of our experiments, $H_2Se$ dictates the concentration of reactant in the system since the lead reactant is fixed. Supersaturation of the reactant leads to rapid homogeneous nucleation, which results in a higher nucleation rate and generally smaller grain sizes. Our observation that particle sizes are larger in the thicker lead films can be attributed to the effect of primary grain growth in the solid thin film. It is possible that the grains grew until they hit an interface where there was a depletion zone and no more lead to consume. This would happen faster in thinner films, resulting in smaller particles on average.

In subsequent experiments, we will focus on slowing down the arrival rate of the precursor, $H_2Se$, with the intent of decreasing the nucleation rate, reducing the favourable kinetics that lead to the formation of $BaSe_3$, and increasing the grain size of PbSe. Decreasing the supersaturation of the reactant would encourage heterogeneous nucleation at the film-substrate interface, bringing us closer to our goal of an epitaxial lead chalcogenide thin film. To remain consistent with our previous experiments, we would keep the $H_2Se$ flow rate constant (75 SCCM) and explore other ways of decreasing the diffusion flux. One way this can be achieved is by decreasing the overall

pressure in the system, which would kinetically slow down the reaction. Another way is to change the gas balance, by mixing $H_2Se$ with some parts argon, thereby diluting the concentration of the reactant. Increasing the growth temperature should also slow down nucleation by making it more difficult for nascent nuclei to stabilize and grow. If these approaches are not effective, it may be necessary to continue tuning the thin film thickness.

We are very interested in how the optoelectronic properties of lead chalcogenide films grown by VLS will compare to those of lead chalcogenide films grown with other techniques, like CBD, MBE, vapour, and liquid growth. We attempted to conduct Hall effect measurements on Sample C, but due the discontinuous network of the PbSe regions, we were not able to get a viable measurement. Once we have obtained a continuous PbSe film, we will try this analysis once again, in addition to conducting responsivity measurements and optical spectroscopy. With the help of collaborators, we will be able to image the interface between the PbSe film and the substrate using tunnel electron microscopy (TEM), which will give us insight into the potential of epitaxial growth. For future samples, we will continue to characterize phase with GIXD, texture with in-plane pole figure analysis, and surface morphology with SEM.

# 6 Conclusion

The ability to grow polycrystalline, epitaxial lead chalcogenide thin films with large crystallites and competitive optoelectronic properties presents a route towards inexpensive, uncooled mid-range IR photon detectors with robust performance. The number of potential applications is vast, including personal IR imagers, enhanced vision systems for automotive applications, sensors for active protection systems (APS), and many others within the military/defense domain [17]. The VLS mechanism circumvents the very slow adsorption of a gas phase into a solid surface by introducing a catalytic liquid alloy phase which can rapidly adsorb a vapor to supersaturation levels, and from which crystal growth can subsequently occur from nucleated seeds at the liquid–solid interface [18]. Large grain sizes and epitaxial layers are predicted to be optimal for improving optoelectronic performance. We have set the stage for further experimentation by demonstrating we can attain a single phase PbSe thin film via VLS growth on an epitaxially matched substrate. We have begun to explore factors that influence diffusion and nucleation rates, such as film thickness and the presence of a capping layer, and these investigations are prompting many more interesting questions.

# References


1. Lovell, D. J. The Development of Lead Salt Detectors. *American Journal of Physics* 37 (5), 467 – 478 (1969).

2. Rogalski, A., and K. Chrzanowski, Infrared devices and techniques. *Opto-Electron. Rev.*10, 111–136 (2002).

3. Rogalski, A. Infrared detectors: an overview. *Infrared Physics & Technology* 43, 187-210 (2002).

4. Capper, P. and C.T. Elliot. *Infrared Detectors and Emitters: Materials and Devices.* Kluwer Academic Publishers: Boston (2001).

5. Johnson, T.H. Cozine, H.T., and B.N. McLean. Lead Selenide Detectors for Ambient Temperature Operation. *Applied Optics* 4 (6), 693-696 (1965).

6. Holloway, H. Thin film IV-VI semiconductor photodiodes. *Physics of Thin Films* 11, 105 (1980).

7. Khokhlov, D. *Lead Chalcogenides: Physics and Applications.* CRC Press: New York (2003).

8. Jonhson, T.H. "Solutions and methods for depositing lead selenide", US Patent 3.178.312 (1965).

9. Grozdanova, I., Najdoskia, M., and S.K. Deyb. A simple solution growth technique for PbSe thin films. *Materials Letters* 38 (1), 28-32 (1999).

10. Okoli, D.N. Growth and Characterization of PbSe Thin Films Prepared By Chemical Bath Deposition Technique. *Res.J.Chem.Sci* 2(8), 72-75 (2012).

11. Diezhandino, J. et *al.* Monolithic integration of spectrally selective uncooled lead selenide detectors for low cost applications. *Appl. Phys. Lett.* 83, 2751 (2003).

12. Moss, T.S. Lead Salt Photoconductors. *Proceedings of the IRE* 43 (12), 1869-1881 (1955).

13. Johnson, T. H., "Lead Salt Detectors and Arrays - PbS and PbSe," Report No. 83-1394, Santa Barbara Research Center, Goleta, CA (1983).

14. Gautier, C., Breton, G., Nouaoura, M., Cambon, M., Charar, S., Averous, M. Sulfide films on PbSe thin layer grown by MBE. *Thin Solid Films* 315 (1-2), 118-122 (1998).

15. Rumianowski, R., Dugdala, R., Jung, W., and Bala, W. Growth of PbSe thin films on Si substrates by pulsed laser deposition method. *Journal of Crystal Growth* 252 (1-3), 250-235 (2003).

16. Kapadia, R. et *al.* A direct thin-film path towards low-cost large-area III-V photovoltaics. *Sci. Rep.* 3, 2275 (2013).

17. Vergara, G. et *al.* Polycrystalline lead selenide: the resurgence of an old infrared detector. *Opto-Electronics Review* 15 (2), 110–117 (2007).

18. Ergen, O. et *al.* Shape-Controlled Synthesis of Single-Crystalline Nanopillar Arrays by Template-Assisted Vapor–Liquid–Solid Process. *Journal of the American Chemical Society* 132 (40), 13972-13974 (2010).